Incipient Damage Detection for Large Area Structures Monitored With a Network of Soft Elastomeric Capacitors Using Relative Entropy

Austin Downey, Mohammadkazem Sadoughi, Simon Laflamme, and Chao Hu

***Abstract*— Structural health monitoring of mesoscale structures is difficult due to their large sizes and often complex geometries. A solution to this challenge lies in the development of sensing skins. Sensing skins are an emerging technology that enables a broad range of sensors and their associated electronics to be integrated onto a single sheet, therefore, reducing the cost and complexity associated with deploying these dense sensor networks onto mesoscale structures. This paper presents a new algorithm for the detection and localization of incipient damage in structures. The algorithm is specialized for a sensing skin consisting of a large area electronic termed as soft elastomeric capacitor. The proposed algorithm utilizes relative entropy to quantify the dissimilarity between one sensor and every other sensor in the network, with more weight placed on the dissimilarities between the sensor of interest and those in its immediate vicinity. The algorithm is data-driven and does not require the healthy condition be known or historical data sets be available to generate damage sensitive indexes. Numerical simulations are used to demonstrate the effectiveness of the data-driven algorithm in both detecting and localizing incipient damage.**

***Index Terms*— Structural health monitoring, capacitive-based sensor, soft elastomeric capacitor, damage detection, relative entropy, full-field strain maps, sensor fusion.**

I. Introduction

LOCALIZATION of damage on mesoscale structural systems, which include full-scale civil, aerospace, and energy structures, is a challenging task, but one that provides real economic incentives arising from the premise of condition-based maintenance [1], [2]. To date, various approaches to damage detection, localization, and quantification on mesoscale structures have been proposed. These approaches can generally be classified into either indirect or direct sensing methods. Indirect sensing of structural systems typically focuses on the vibration monitoring of the systems where damage is localized through the use of sophisticated data analysis or model-assisted damage detection [3]. While vibration monitoring is capable of detecting damage in mesoscale structures using a limited number of sensors, the localization of damage is an arduous task. In contrast to the indirect sensing approaches, direct sensing approaches function through the direct measurements of a structure using discrete, often strain transducing sensors [4]. Distributed dense sensor networks (DSNs) can be deployed for direct damage sensing of large surfaces. While the use of DSNs offers excellent damage localization capabilities, the technical (e.g., signal cross-talk and wire management) and economic (e.g., installation and data processing costs) trade-offs make deploying a high number of traditional, individually mounted sensors challenging [5]. In the case where damage of sufficient magnitude forms directly under a sensor, this damage [6] is often detectable using simple threshold style algorithms [7]. However, the detection of incipient damage (early stage damage of low magnitude) is more complex as its signature contained in the sensor signal is weak and concealed by sensor noise. Data-driven techniques based on statistical methods have been used to detect incipient damage in various engineered systems [8]–[10].

One solution to the deployment of DSNs is enabled by recent advances in sensor technologies that allow for all the required sensors, electronics, and communications to be mounted onto a single flexible substrate, creating a sensing skin [11]–[14]. These sensing skins, also termed sensing sheets or electronic artificial skins, mimic biological skin in that they are capable of detecting and localizing damage over the structure's global area. In this work, a previously proposed sensing skin consisting of a network of large area sensors, termed soft elastomeric capacitor (SEC), is used as the sensing skin [15]. The SEC is a low cost and robust large area sensor that transduces a change in a structure's geometry into a measurable change in capacitance. The detection of damage within the area monitored by the SEC-based sensing skin has been investigated both numerically and experimentally through various approaches. These include the spatio-temporal comparison of sensor responses [16] and the monitoring of changes in full-field strain maps [17]. In this paper, we propose an algorithm termed spatial damage index (SDI) that leverages

Manuscript received June 27, 2018; revised August 8, 2018; accepted August 29, 2018. Date of publication August 31, 2018; date of current version October 10, 2018. This work was supported by the National Science Foundation under Grant CNS-1566579, Grant ECCS-1611333, Grant 1069283, and Grant 1069283. The associate editor coordinating the review of this paper and approving it for publication was Dr. Chao Tan. *(Corresponding author: Austin Downey.)*

A. Downey is with the Department of Mechanical Engineering, University of South Carolina, Columbia, SC 29201 USA (e-mail: adowney2@cec.sc.edu).

M. Sadoughi and C. Hu are with the Department of Mechanical Engineering, Iowa State University, Ames, IA 50010 USA.

S. Laflamme is with the Department of Civil, Environmental, and Construction Engineering, Iowa State University, Ames, IA 50010 USA, and also with the Department of Electrical and Computer Engineering, Iowa State University, Ames, IA 50010 USA.

Digital Object Identifier 10.1109/JSEN.2018.2868135

the network configuration of the SEC-based sensing skin in combination with the kriging interpolation method to generate spatial damage maps that provide improved damage detection capabilities over existing gradient-based spatial damage detection methods. Kriging is utilized to generate full-field strain maps that contain both the expected value and its variance at each point of interest within the monitored area.

The proposed SDI algorithm utilizes the relative entropy between two probability density functions (PDFs) to quantify the dissimilarity between the signal of one sensor and that of every other sensor in the network, with more weight placed on the dissimilarities between the sensor of interest and those in its immediate neighborhood. The use of relative entropy, often based on the Kullback-Leibler divergence (KLD), has been shown to improve the detection of incipient damage over the monitoring of changes in signals (e.g., shifts in signal means or variances) directly [18]. KLD has found uses for crack detection in a nickel-based alloy plate [8], anomaly detection in electric motors [19], and fault detection in composite wing structures [20]. SDI provides a spatially distributed damage index that is obtained directly from the data (i.e., data-driven) without the use of black boxes or historical data sets. SDI calculates a damage sensitive index for any given location in the monitored section of a structure by taking the L1-norm of multiple KLD values. Each of these KLD values is obtained by comparing the PDF of the kriging estimated strain at the point of interest with that at the same point when one SEC is removed from the training set. SDI creates a full-field map of damage sensitive indexes by recursively solving for each KLD value at all the points of interests. These damage sensitive indexes can be interpreted as damage when compared to a proper baseline (i.e. healthy condition) [21]. This work presents a numerical investigation of the SDI algorithm for detecting incipient damage on a reinforced concrete beam.

II. Background

This section provides a review of the SEC sensor and the SEC-based sensing skin, followed by an overview of kriging.

A. SEC-Based Sensing Skin

The SEC-based sensing skin is based on a network of densely deployed SECs. The SEC is a low-cost, robust, and highly scalable thin-film strain sensor that consists of a parallel plate capacitor. For a given change in a monitored structure's geometry of (i.e., strain), the SEC transduces a measurable change in its capacitance. An SEC, presented in figure 1(a) with its key components annotated, is constituted from an SEBS block co-polymer arranged in three layers where the inner layer (dielectric) is filled with TiO_2 to increase both its durability and permittivity while the outer layers (conductors) are doped with carbon black to both provide conductive pathways and increase the sensor's resiliency to weathering. Manufacturing of the SEC is covered in more detail in [15]. A model that relates change in a sensor's capacitance (C) to a change in the monitored structure geometry (i.e. strain) can be derived from the parallel plate capacitor equation:

$$C = e_0 e_r \frac{A}{h} \tag{1}$$

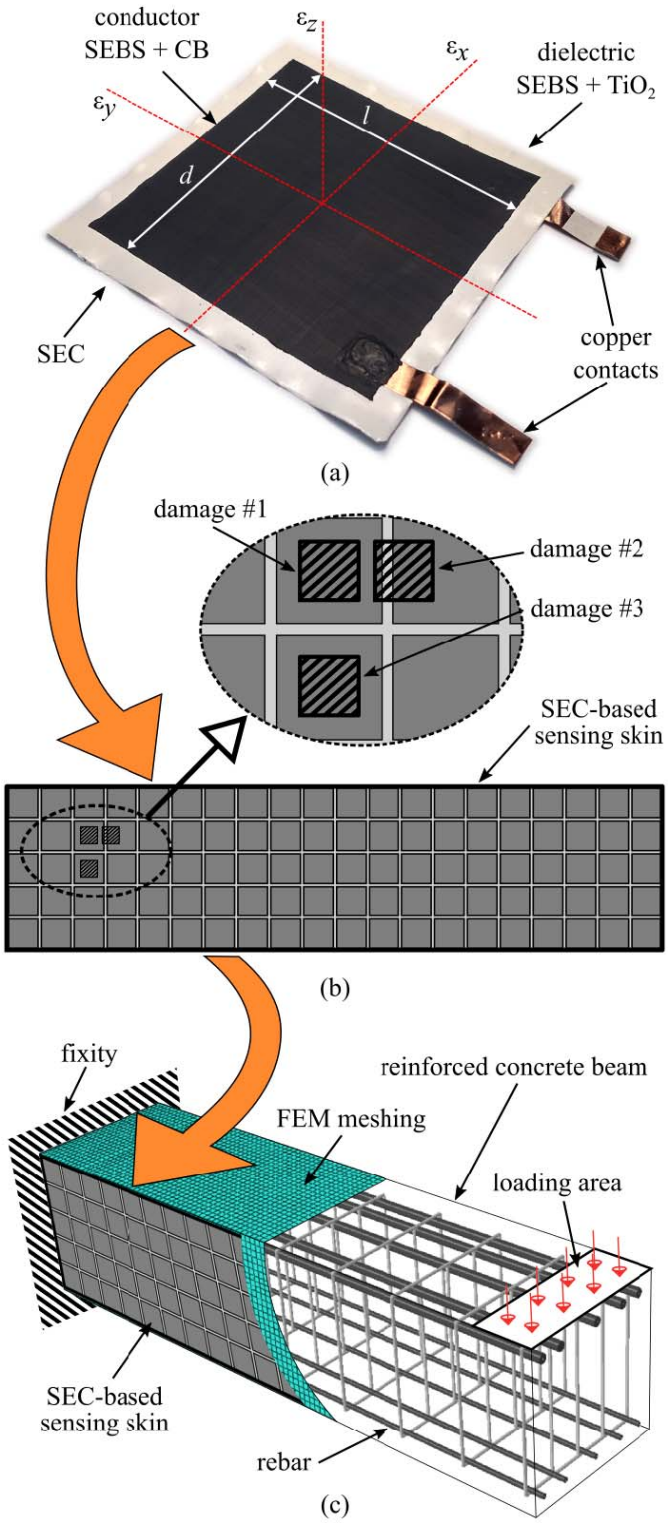

Fig. 1. SEC-based sensing skin for the monitoring of mesoscale structures showing the: (a) SEC sensor with key components and axes annotated; (b) layout of the SEC-based sensing skin used in this study including the 3 damage cases investigated; (c) SEC-based sensing skin deployed onto the side of a reinforced cantilever concrete beam.

where $e_0 = 8.854$ pF/m is the vacuum permittivity, e_r is the polymer's relative permittivity, $A = d \cdot l$ is the sensor area of width d and length l (as annotated in Figure 1(a)), and h is the thickness of the dielectric. Assuming small strains in the substrate and a plane stress condition in the sensor,

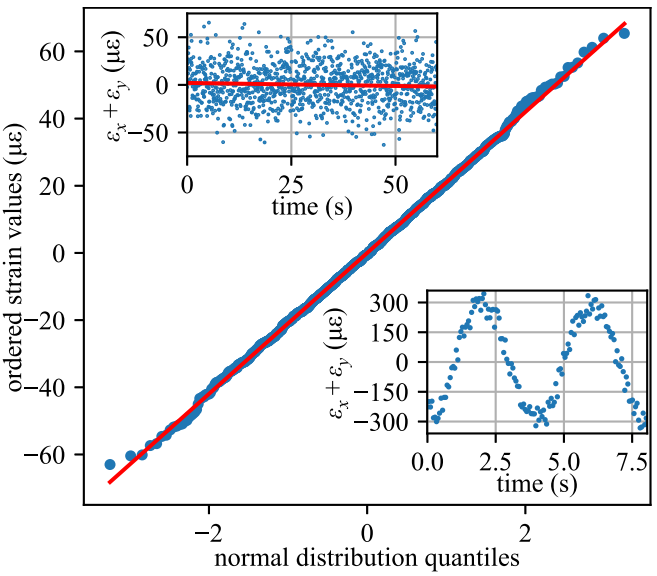

Fig. 2. Q-Q plot of SEC sensor signal compared to a normal distribution along with the static temporal data from which this data was taken (upper inset) and the sensor's response to a sinusoidal load (lower inset).

equation (1) can be written as a change in capacitance (ΔC):

$$\frac{\Delta C}{C} = \lambda(\varepsilon_x + \varepsilon_y) \tag{2}$$

where ν is the sensor material's Poisson's ratio taken as $\nu \approx 0.49$ [22], with $\lambda = 1/(1-\nu) \approx 2$ representing the gauge factor of the sensor. A key advantage of the SEC is its capability to measure the additive strain of a structure, as shown in equation (2). Previously reported experimental data for an SEC is presented in figure 2. The main figure consists of a quantile-quantile (Q-Q) plot demonstrating that the noise of an SEC signal can be effectively estimated by a normal distribution with a standard deviation of $\sigma = 32\ \mu\varepsilon$. The upper inset shows the static signal from which this data was extracted, while the lower inset shows a sensor response for the SEC under a dynamic load. More details regarding the quantification of SEC noise can be found in [23].

Figure 1(b) presents an SEC-based sensing skin, consisting of a network of densely deployed SECs mounted onto the surface of a structure, as shown in figure 1(c). A fully realized SEC-based sensing skin would consist of a flexible substrate (e.g., Kapton) with all the required electronics for power management, data acquisition, and communications, embedded onto the substrate. For more detail on the proposed sensing skin, the interested reader is referred to [17]. To further leverage the network of SECs, the geometry of an SEC can be fused into the strain signal using the previously proposed technique presented in [23].

B. Universal Kriging

Kriging is a method of spatial interpolation for which the interpolated values are modeled by a Gaussian process [24]. Importantly for this work, kriging provides both an interpolated value at any location within the spatial grid and its associated confidence interval that represent the uncertainty of the interpolation. Kriging predicts the value of a function at a point of interest by computing a spatially weighted average of the training points in the neighborhood. The function under consideration can be modeled as $\mathbf{Z}(x) = \mu(x) + \epsilon(x)$, where $\mathbf{Z}(x)$ is the real value at location x and $\mu(x)$ is the expected constant mean value of the process and $\epsilon(x)$ denotes the small-scale spatial variation in the process. However, in situations where the mean value of the function varies smoothly, as it is generally the case with strain fields, universal kriging (UK) is preferred [25]. A kriging estimated value at the point of interest, $\hat{z}(x_0)$, can be expressed as the sum of the drift drifting mean value ($\hat{m}$) plus the residual ($\hat{e}$):

$$\hat{z}(x_0) = \hat{m}(x_0) + \hat{e}(x_0) \tag{3}$$

where the drift term $\hat{m}$ is fit onto an assumed trend term using linear regression. This work utilizes the regional linear drift trend to estimate the mean value at x_0, however other terms including linear, polynomial, and point logarithmic [26] could also be used. Equation 3 can be written in a matrix notation:

$$\hat{z}(x_0) = \mathbf{q}_0^{\mathrm{T}} \cdot \hat{\boldsymbol{\beta}} + \boldsymbol{\lambda}_0^{\mathrm{T}} \cdot \mathbf{e} \tag{4}$$

where $\mathbf{q}_0$ is a vector of the predictors at x_0, $\hat{\boldsymbol{\beta}}$ is a vector that contains the estimated drift term coefficients, $\boldsymbol{\lambda}_0$ is a vector of kriging weights determined by the covariance function, and $\mathbf{e}$ is a vector that contains all the regression residuals. The covariance matrix ($\mathbf{C}$) is estimated using the power variogram model expressed as $s \cdot d^{\alpha} + n$, where s is a scaling factor, α is the exponent (between 1 and 1.99), and n is the nugget term that effectively takes up "noise" in the measurement [24]. The variance of the kriging estimate at the point of interest can then be calculated by:

$$\sigma^2(x_0) = n - \mathbf{c}_0^{\mathrm{T}} \cdot \mathbf{C}^{-1} \cdot \mathbf{c}_0 + (\mathbf{q}_0 - \mathbf{q}^{\mathrm{T}} \cdot \mathbf{C}^{-1} \cdot \mathbf{c}_0)^{\mathrm{T}} \cdot (\mathbf{q}^{\mathrm{T}} \cdot \mathbf{C}^{-1} \cdot \mathbf{q})^{-1} \cdot (\mathbf{q}_0 - \mathbf{q}^{\mathrm{T}} \cdot \mathbf{C}^{-1} \cdot \mathbf{c}_0) \tag{5}$$

where $\mathbf{c}_0$ is a vector consisting of the residuals between the points of interests and the known data points. UK can create a near continuous interpolation of a sampled process, given that various points of interest are sampled with sufficient density. This work utilized PyKrige for the development and solving of the UK interpolation models [27], itself based on the work found in [24].

C. Kullback-Leibler Divergence

The Kullback-Leibler divergence (also called relative entropy) is a method for quantifying the dissimilarity between two PDFs [8]. For distributions P and Q of two continuous random variables, with the respective densities denoted as p and q, the KLD is defined to be the following integral

$$D_{\mathrm{KL}}(P||Q) = \int_{-\infty}^{\infty} p(x) \cdot \log \frac{p(x)}{q(x)} dx \tag{6}$$

However, when dealing with two Gaussian distributions, as generated by equations 4 and 5, the KLD of the Gaussian distributions (P and Q) can be represented by their respective means and variances (μ_p, σ_p, μ_q and σ_q). Correspondingly, equation 6 becomes:

$$D_{\mathrm{KL}}(P||Q) = \log\left(\frac{\sigma_q}{\sigma_p} + \frac{\sigma_p^2 + (\mu_p - \mu_q)^2}{2\sigma_q^2} - \frac{1}{2}\right) \tag{7}$$

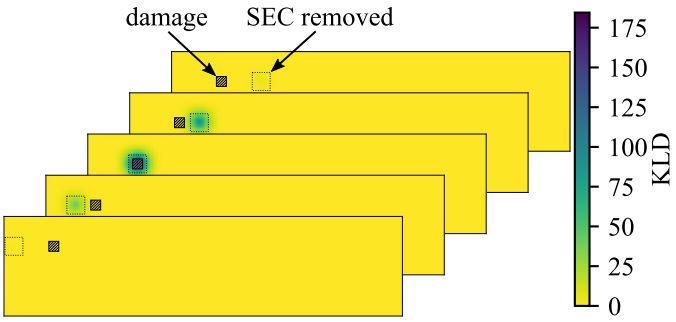

Fig. 3. Full-field KLDs for five different Qs, each with a different SEC removed from the kriging training set, showing KLDs increases in the presence of strain map anomalies (e.g., damage).

therefore simplifying the computational processes required for the calculation of the KLD.

III. Methodology

This section first introduces the proposed algorithm and then discusses the numerical validation procedure used in this work.

A. SDI Algorithm

This work proposes the novel SDI algorithm for the creation of full-field damage indicator maps. The SDI algorithm generates these damage indicator maps through a systematic approach that progressively calculates the KLD between a kriging interpolated model developed using all sensors in the sensing skin and a model developed with one sensor removed from the training set used to build the kriging model. Let us consider an SEC-based sensing skin with n sensors. SDI starts by first calculating the probability distribution P characterized with μ_p and σ_p from equations 4 and 5 for the training set that considers all n SECs. Thereafter, n different Q probability distributions are calculated for each of the points of interest. Each Q probability distribution is developed from a training set consisting of $n-1$ SECs where the removed SEC is changed for each successive calculation. The distribution Q is also represented by its mean and variance values (μ_q and σ_q) as calculated using equations 4 and 5. After, the KLD for each point of interest is calculated between P and Q using equation 7. Figure 3 demonstrates how the KLD increases between P and the respective Q at the points of interest around the damage when an SEC is removed close to or exactly above the damage. Next, the SDI algorithm calculates the L1-norm of the n KLDs at each spatial point of interest. Lastly, the L1-norm lengths are plotted to generate the spatially distributed damage sensitive indexes. To summarize, the SDI algorithm follows a direct six step process:

1) Strain measurements are obtained from each SEC.
2) A full-field strain map of P is developed by using all n sensors to train the kriging model.
3) n full-field strain maps of Q are generated where each strain map is generated by ignoring one of the SECs.
4) For each point of interest, n KLDs are generated between P and the n unique Qs.
5) The length (L1-norm) of the KLDs is obtained for each location of interest.
6) The L1-norm lengths are plotted to generate the spatially distributed damage sensitive indexes.

B. Numerical Validation

The finite element analysis (FEA) model used for the simulations is presented in figure 1(c). It consists of a $2 \times 0.5 \times 0.5$ meter reinforced cantilever concrete beam loaded at its tip. The beam was constructed in Abaqus using 72,306 eight-node brick elements with reduced integration [28]. The FEA meshing is visible in figure 1(c). The loading cases considered are such that the beam remains linear. Three damage locations are used in this work and are presented in the subset of figure 1(b). These damage locations, each introduced into the FEA model as a reduction in the concrete's stiffness, protrude all the way through the beam. Damage cases were selected to investigate damage that forms directly under a sensor (damage location #1), under two sensors (damage location #2), and close to the neutral axis of the beam where strain levels are lower (damage location #3). The SEC data is obtained by taking the average additive strain under each sensor, applying noise from a normal distribution ($\sigma = 32\ \mu\varepsilon$), and fusing the sensor geometry into the strain signals.

For each damage location, 156 different combinations of damage and loading cases were considered. These combinations were constituted by pairing each of the 12 damage cases with each of the 12 loading cases (plus one healthy case). These results are first presented as damage index maps for a few selected loading/damage case combinations. The loading levels and damage levels, introduced as relative changes $\Delta\%$ of the concrete stiffness value in the damage area, are presented in table I. The damage detection maps obtained by the SDI algorithm are compared to those obtained by second-order Laplace and Gaussian filters to show the enhanced capabilities of SDI over these accepted techniques. A grid measuring 100×400 for the points of interest was solved for by SDI.

Subsequently, the metrics for the detection and localization of damage are considered. The damage is considered to be properly detected and localized if the maximum L1 length of the damage is both at the location of the damage and higher than any L1 distance calculated using the healthy beam case. The use of this threshold index eliminates the possibility of false positives (i.e. damage that is correctly localized but only as a function of the signal noise). In the case of localization, the damage is considered to be correctly localized if the max damage index obtained by the SDI algorithm is within 0.05 meters from the damage. Calculations for the probability of detection (POD) for each of the loading/damage case combinations is achieved by generating 50 noise cases for each case combination and dividing the number of noise cases where the damage is correctly detected and localized by the total number of noise cases.

IV. Results

The spatially distributed damage sensitive indexes generated using the SDI algorithm are presented in figures 4-6. These figures report the SEC-measured strain values on the leftmost column and the results by the SDI algorithm on the

TABLE I
LOADING AND DAMAGE CASES USED IN THE NUMERICAL SIMULATIONS

	case #1	case #2	case #3	case #4	case #5	case #6	case #7	case #8	case #9	case #10	case #11	case #12
loading (kNs)	735	1114	1493	1872	2250	2629	3008	3387	3766	4145	4525	4903
damage (Δ%)	-65	-68	-71	-74	-77	-80	-83	-85	-88	-91	-94	-97
signal to noise ratio	1.36	1.83	2.37	3.01	3.78	4.66	5.63	6.69	7.81	8.98	10.21	11.49

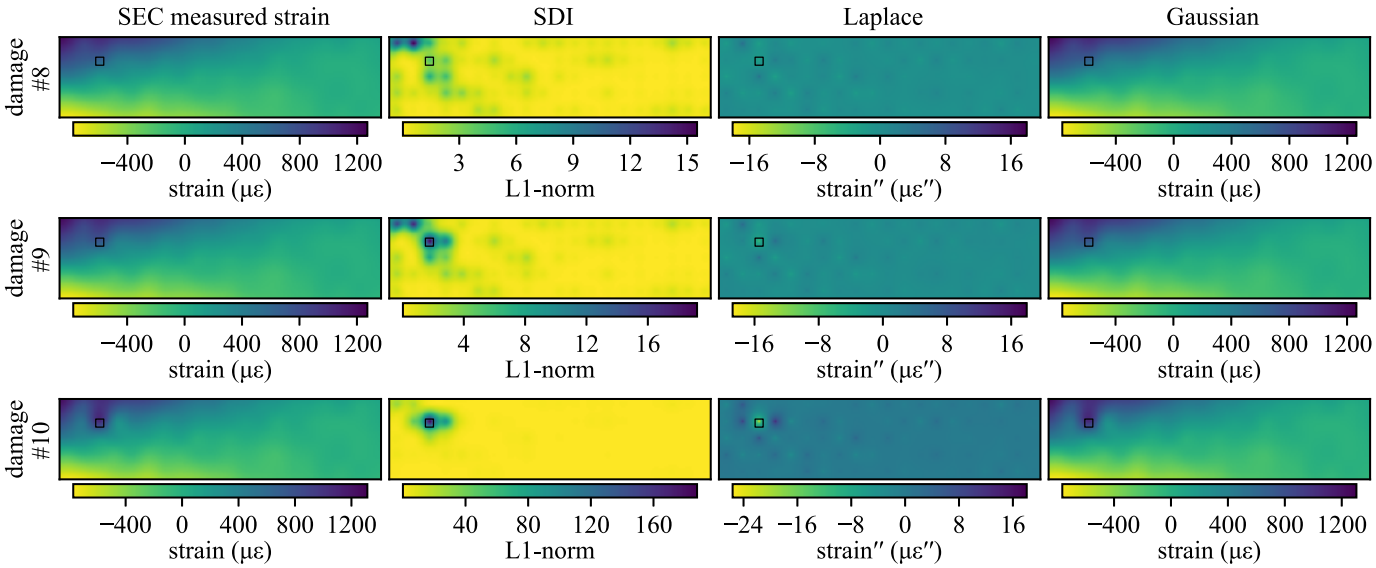

Fig. 4. Numerical validation of the SDI algorithm for damage location #1 under loading case #12 showing (by column) the SEC measured strain maps, the SDI generated damage indexes, the Laplace transformation, and the Gaussian transformation for three different damage cases.

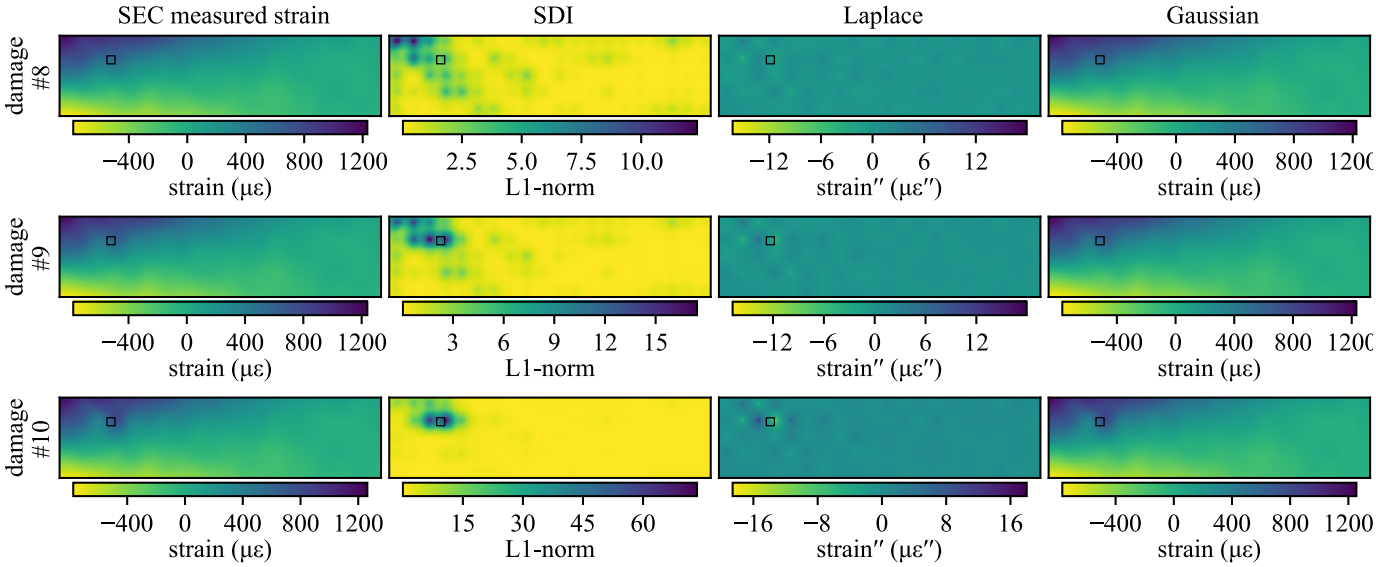

Fig. 5. Numerical validation of the SDI algorithm for damage location #2 under loading case #12 showing (by column) the SEC measured strain maps, the SDI generated damage indexes, the Laplace transformation, and the Gaussian transformation for three different damage cases.

center-left column. Additionally, the results for the gradient-based image filtering techniques (Laplace and Gaussian transformations) are reported in the center-right and rightmost columns. The colorbars report each subfigure's min and max values. Figure 4, reporting the results for damage location #1, shows that, for lower damage cases (i.e. damage cases #1-8) under this loading condition, the SDI algorithm tends to identify damage along the top edge of the beam where the strain values are the greatest. However, when the damage level increases to damage case #9, the SDI algorithm correctly localizes the incipient damage. This damage case is not notably detectable through the direct inspection of the measured strain map, the Laplace transformation, or the Gaussian transformation. Increasing the severity of damage to case #10, the SDI algorithm detects the damage. While the Laplace transformation can also detect damage at this stage,

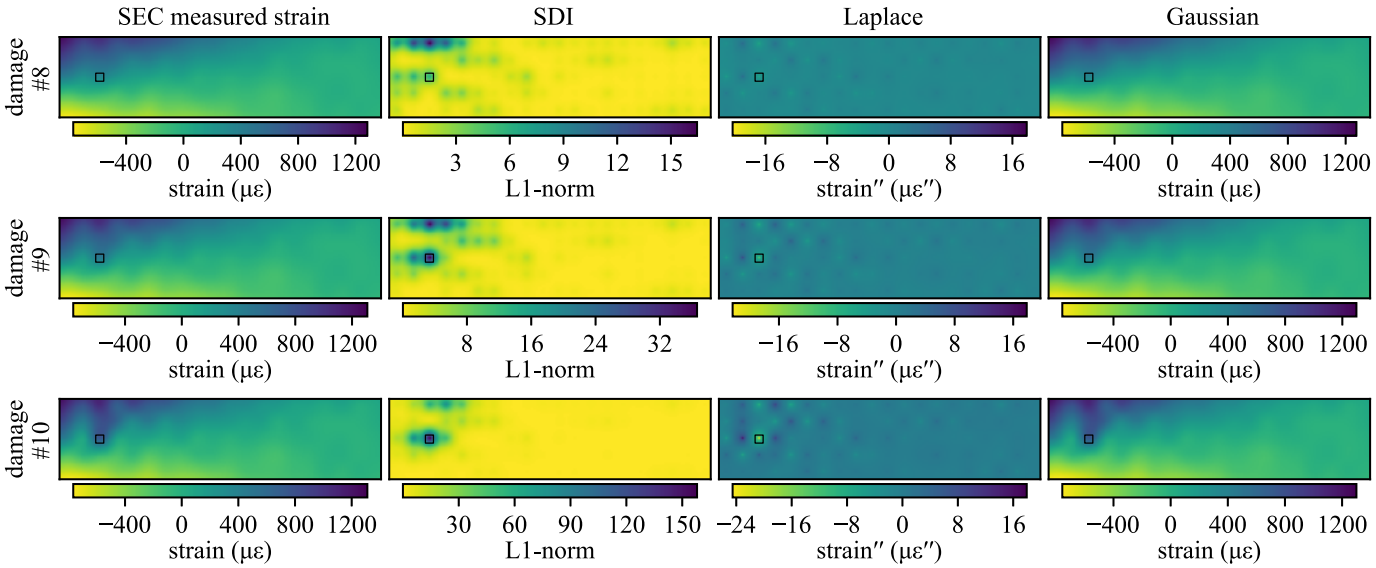

Fig. 6. Numerical validation of the SDI algorithm for damage location #3 under loading case #12 showing (by column) the SEC measured strain maps, the SDI generated damage indexes, the Laplace transformation, and the Gaussian transformation for three different damage cases.

results are much less evident than those from the SDI algorithm. Furthermore, damage detection from the strain map or Gaussian transformation is still uncertain and would require further signal post-processing.

Figure 5 report the results produced by the SDI algorithm for a damage (location #2) that sits in between the two SEC sensors. As observed in figure 4, for low levels of damage the SDI algorithm tends to localize damage in the areas of high strain. However, as the damage increases in severity, the algorithm is able to correctly detect and locate the damage. In comparison to damage location #1, damage location #2 has considerably more spread in its estimated damage location. This is attributed to the damage not being completely covered by a single sensor, but rather directly affecting two sensors as seen in figure 1(b). Similar to the results for damage location #1, the SDI algorithm outperforms both the Laplace and Gaussian transformations in all cases. While the Laplace transformation was able to detect and localize the damage in damage case #10, results are also less evident than those from the SDI algorithm. Lastly, damage location #3 is considered in figure 5. This damage, located near the neutral axis of the beam, sees significantly less strain and therefore lower signals at the location of the damage. However, the damage can still be correctly located by the SDI algorithm, given that the damage is severe enough. As before, the SDI algorithm outperform both the Laplace and Gaussian transformations.

The peak L1-norms for three damage cases are presented in figure 7 for loading case #12 under damage location #1. The left-hand side of the subfigures reports the peak damage indexes for the healthy condition. Considering the maximum healthy value as the threshold for damage detection, the right-hand side of figures (a)-(c) presents the max L1-norm distance of the damage cases #7, #9, and #10. Figure 7(a) presents a condition that only correctly localizes the damage 7 out of 50 times, however, this case does not generate any L1-norm distances greater than that generated by the healthy data and as such does not correctly identify any damage, resulting in

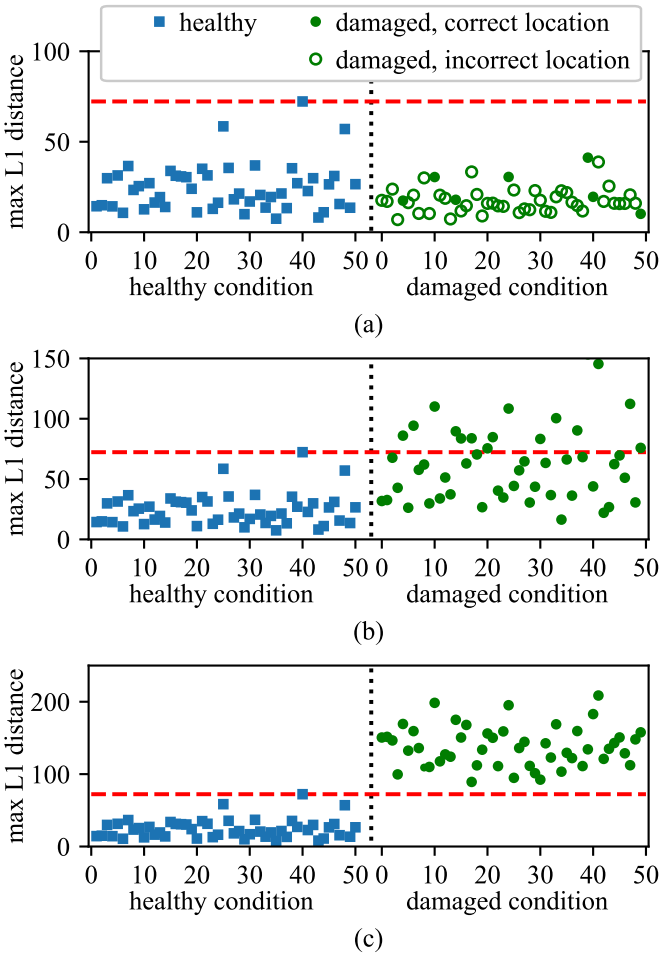

Fig. 7. Max damage index values showing the relationship between the healthy and damage values, including noise cases with correct/incorrect damage localization, for loading case #12 under damage case: (a) #7; (b) #9; and (c) #10.

a POD of 0. In comparison, figure 7(b) correctly localizes the damage for every noise case considered. However, due to the relatively high level of noise in the SECs, only 16 cases

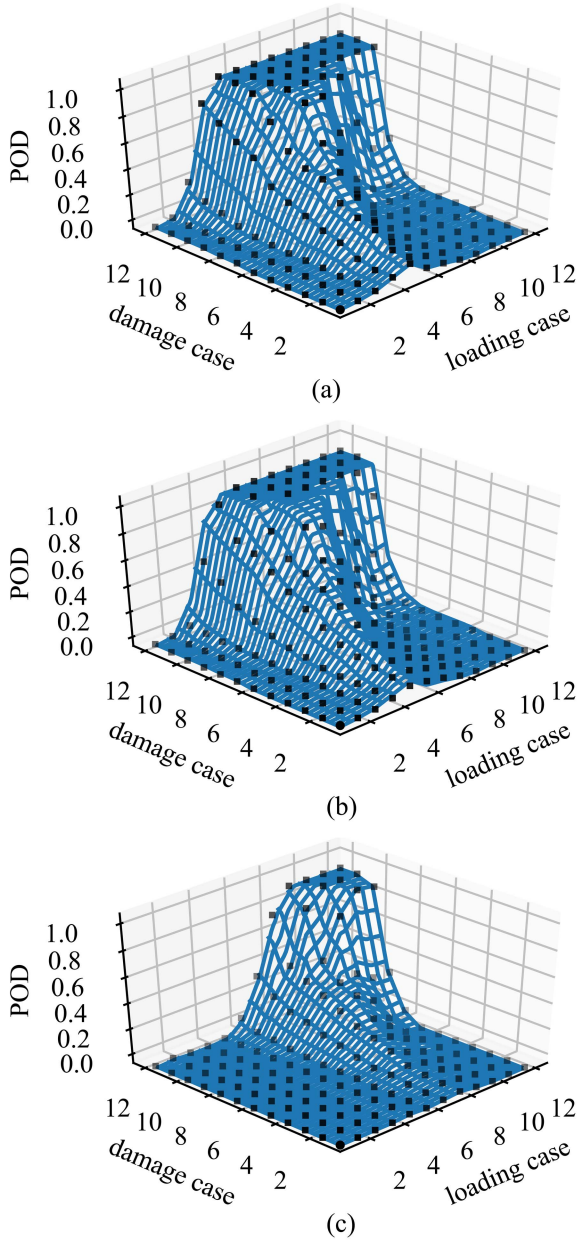

Fig. 8. POD results for damage location: (a) #1; (b) #2; and (c) #3.

fall above the minimum threshold set by the healthy condition and a POD of 0.32 is obtained. An example of this situation can be seen in figure 4 for damage case #9 where the maximum L1 distance correctly locates the damage. However, this value (17.5) falls below the max value obtained from the 50 samples of the healthy state. Lastly, figure 7(c) shows a case in which the damage is correctly detected for every noise case, resulting in a POD of 1. Figure 8 reports the POD values for each of the loading/damage case combinations. Generally, given a severe enough damage and sufficient loading force, the SDI algorithm is shown to be capable of accurately and repeatably detecting and localizing damage within the area monitored by the sensing skin. The reduction in the POD for the relatively low damage cases with an increase in the applied loading forces is a result of increasing strain values along the top of the beam, as discussed before and shown in figures 4-6.

V. Conclusion

An algorithm for damage detection and localization over the surfaces of mesoscale structures monitored by a sensing skin has been proposed. The sensing skin used in this work was based on a large area electronic, termed soft elastomeric capacitor, that is capable of covering a large area at a low cost. When arranged in a network configuration, these sensors are capable of reconstructing the full-field additive strain maps of the structure. The proposed spatial damage index (SDI) algorithm enhances the damage detection and localization capabilities of the sensing skin by leveraging the sensor network, where the KLD is progressively calculated at each point in the monitored structure between two kriging-developed strain maps. The first of these kriging strain maps is built using data from all SEC sensors while the set of second strain maps is calculated by progressively removing one sensor from the training set used to build the kriging model. Thereafter, multiple KLDs are calculated at each point of interest between the strain map generated using all the sensors and each of the strain maps generated with a single sensor extracted from the data set used for training the kriging model. Lastly, the L1-norm of the KLD values is calculated at each point of interest, therefore creating a spatially distributed damage sensitive index. A numerical validation, performed on a reinforced cantilever concrete beam, showed that the proposed SDI algorithm was capable of detecting incipient damage before the damage severity becomes detectable by a Laplace or Gaussian transform. Overall, the proposed algorithm's performance, combined with the high scalability of the sensing skin, makes the technology a promising candidate for structural health monitoring of mesoscale structures. Future work includes scaled and full-scale experimental testing to validate the proposed algorithm under time-varying environmental conditions (e.g., temperature and humidity).

Acknowledgment

Any opinions, findings, and conclusions or recommendations expressed in this material are those of the authors and do not necessarily reflect the views of the National Science Foundation.

References

[1] V. Giurgiutiu, A. Zagrai, and J. Bao, "Damage identification in aging aircraft structures with piezoelectric wafer active sensors," *J. Intell. Mater. Syst. Struct.*, vol. 15, nos. 9–10, pp. 673–687, Sep. 2004, doi: 10.1177/1045389x04038051.

[2] J. P. Lynch, C. R. Farrar, and J. E. Michaels, "Structural health monitoring: technological advances to practical implementations [scanning the issue]," *Proc. IEEE*, vol. 104, no. 8, pp. 1508–1512, Aug. 2016, doi: 10.1109/jproc.2016.2588818.

[3] N. Cavalagli, G. Comanducci, and F. Ubertini, "Earthquake-induced damage detection in a monumental masonry bell-tower using long-term dynamic monitoring data," *J. Earthq. Eng.*, pp. 1–24, Aug. 2017, doi: 10.1080/13632469.2017.1323048.

[4] M. Perry, J. McAlorum, G. Fusiek, P. Niewczas, I. McKeeman, and T. Rubert, "Crack monitoring of operational wind turbine foundations," *Sensors*, vol. 17, no. 8, p. 1925, Aug. 2017, doi: 10.3390/s17081925.

[5] M. A. Rumsey and J. A. Paquette, "Structural health monitoring of wind turbine blades," in *Smart Sensor Phenomena, Technology, Networks, and Systems*, W. Ecke, K. J. Peters, and N. G. Meyendorf, Eds. Bellingham, WA, USA: SPIE, Mar. 2008, doi: 10.11172F12.778324.

[6] B. R. Loyola, V. L. Saponara, K. J. Loh, T. M. Briggs, G. O'Bryan, and J. L. Skinner, "Spatial sensing using electrical impedance tomography," *IEEE Sensors J.*, vol. 13, no. 6, pp. 2357–2367, Jun. 2013, doi: 10.1109/jsen.2013.2253456.
[7] J. P. Lynch, A. Sundararajan, K. H. Law, A. S. Kiremidjian, and E. Carryer, "Embedding damage detection algorithms in a wireless sensing unit for operational power efficiency," *Smart Mater. Struct.*, vol. 13, no. 4, pp. 800–810, Jun. 2004, doi: 10.1088/0964-1726/13/4/0180.
[8] J. Harmouche, C. Delpha, D. Diallo, and Y. L. Bihan, "Statistical approach for nondestructive incipient crack detection and characterization using kullback-leibler divergence," *IEEE Trans. Rel.*, vol. 65, no. 3, pp. 1360–1368, Sep. 2016, doi: 10.1109/tr.2016.2570549.
[9] Z. Rahman, H. Ohba, T. Yoshioka, and T. Yamamoto, "Incipient damage detection and its propagation monitoring of rolling contact fatigue by acoustic emission," *Tribol. Int.*, vol. 42, no. 6, pp. 807–815, Jun. 2009, doi: 10.1016/j.triboint.2008.10.014.
[10] L. Frosini, C. Harlişca, and L. Szabó, "Induction machine bearing fault detection by means of statistical processing of the stray flux measurement," *IEEE Trans. Ind. Electron.*, vol. 62, no. 3, pp. 1846–1854, Mar. 2015, doi: 10.1109/tie.2014.2361115.
[11] S. Khan, L. Lorenzelli, and R. S. Dahiya, "Technologies for printing sensors and electronics over large flexible substrates: A review," *IEEE Sensors J.*, vol. 15, no. 6, pp. 3164–3185, Jun. 2015, doi: 10.1109/jsen.2014.2375203.
[12] B. Glisic, Y. Yao, S.-T. E. Tung, S. Wagner, J. C. Sturm, and N. Verma, "Strain sensing sheets for structural health monitoring based on large-area electronics and integrated circuits," *Proc. IEEE*, vol. 104, no. 8, pp. 1513–1528, Aug. 2016, doi: 10.1109/jproc.2016.2573238.
[13] M. Ahmed, I. E. Gonenli, G. S. Nadvi, R. Kilaru, D. P. Butler, and Z. Celik-Butler, "MEMS sensors on flexible substrates towards a smart skin," in *Proc. IEEE Sensors*, Oct. 2012, pp. 1–4, doi: 10.1109/icsens.2012.6411363.
[14] Y.-L. Park, B.-R. Chen, and R. J. Wood, "Design and fabrication of soft artificial skin using embedded microchannels and liquid conductors," *IEEE Sensors J.*, vol. 12, no. 8, pp. 2711–2718, Aug. 2012, doi: 10.1109/jsen.2012.2200790.
[15] S. Laflamme, M. Kollosche, J. J. Connor, and G. Kofod, "Robust flexible capacitive surface sensor for structural health monitoring applications," *J. Eng. Mech.*, vol. 139, no. 7, pp. 879–885, 2013, doi: 10.1061/(asce)em.1943-7889.00005300.
[16] X. Kong, J. Li, W. Collins, C. Bennett, S. Laflamme, and H. Jo, "A large-area strain sensing technology for monitoring fatigue cracks in steel bridges," *Smart Mater. Struct.*, vol. 26, no. 8, p. 085024, Jul. 2017, doi: 10.1088/1361-665x/aa75ef.
[17] A. Downey, S. Laflamme, and F. Ubertini, "Experimental wind tunnel study of a smart sensing skin for condition evaluation of a wind turbine blade," *Smart Mater. Struct.*, Oct. 2017, doi: 10.1088/1361-665X/aa9349.
[18] J. Zeng, U. Kruger, J. Geluk, X. Wang, and L. Xie, "Detecting abnormal situations using the Kullback-divergence," *Automatica*, vol. 50, no. 11, pp. 2777–2786, Nov. 2014, doi: 10.1016/j.automatica.2014.09.005.
[19] A. Giantomassi, F. Ferracuti, S. Iarlori, G. Ippoliti, and S. Longhi, "Electric motor fault detection and diagnosis by kernel density estimation and kullback-divergence based on stator current measurements," *IEEE Trans. Ind. Electron.*, vol. 62, no. 3, pp. 1770–1780, Mar. 2015, doi: 10.1109/tie.2014.2370936.
[20] J. M. Nichols, M. Seaver, S. T. Trickey, L. W. Salvino, and D. L. Pecora, "Detecting impact damage in experimental composite structures: An information-theoretic approach," *Smart Mater. Struct.*, vol. 15, no. 2, pp. 424–434, Feb. 2006, doi: 10.1088/0964-1726/15/2/023.
[21] K. Worden, C. R. Farrar, G. Manson, and G. Park, "The fundamental axioms of structural health monitoring," *Proc. Roy. Soc. A, Math., Phys. Eng. Sci.*, vol. 463, no. 2082, pp. 1639–1664, Apr. 2007, doi: 10.1098/rspa.2007.1834.
[22] A. Wilkinson, M. Clemens, and V. Harding, "The effects of SEBS-*g*-maleic anhydride reaction on the morphology and properties of polypropylene/PA6/SEBS ternary blends," *Polymer*, vol. 45, no. 15, pp. 5239–5249, Jul. 2004, doi: 10.1016/j.polymer.2004.05.033.
[23] A. Downey, M. Kazem, S. Laflamme, and C. Hu, "Fusion of sensor geometry into additive strain fields measured with sensing skin," *Smart Mater. Struct.*, vol. 27, no. 7, p. 075033, May 2018, doi: 10.1088/1361-665x/aac4cd.
[24] P. K. Kitanidis, *Introduction to Geostatistics Applications in Hydrogeology*. Cambridge, U.K.: Cambridge Univ. Press, 1997.
[25] T. Hengl, G. B. Heuvelink, and A. Stein, "A generic framework for spatial prediction of soil variables based on regression-kriging," *Geoderma*, vol. 120, nos. 1–2, pp. 75–93, May 2004, doi: 10.1016/j.geoderma.2003.08.018.
[26] M. J. Tonkin and S. P. Larson, "Kriging water levels with a regional-linear and point-logarithmic drift," *Ground Water*, vol. 40, no. 2, pp. 185–193, Mar. 2002, doi: 10.1111/j.1745-6584.2002.tb02503.x.
[27] rth, bsmurphy, mjziebarth, and basaks. (2018). *Pykrige: Kriging Toolkit for Python*. [Online]. Available: https://github.com/bsmurphy/PyKrige/graphs/contributors
[28] *ABAQUS/Standard Analysis User's Manual*, Hibbit, Karlsson, Sorensen Inc., Birmingham, AL, USA, 2007.

Austin Downey received the B.S. degree in civil engineering from Iowa State University Ames, IA, USA, in 2014, and the Ph.D. degree in engineering mechanics and the Ph.D. degree in wind energy science engineering and policy from Iowa State University in 2018, where he was an NSF-IGERT Fellow. He is currently an Assistant Professor of Mechanical Engineering with the University of South Carolina, Columbia, SC, USA. His research interests include multifunctional materials, large area sensors, and hybrid dense sensor networks.

Mohammadkazem Sadoughi received the B.S. degree in mechanical engineering from the University of Mazandaran, Mazandaran, Iran, in 2010, and the M.S. degree in mechanical engineering from the University of Tehran, Tehran, Iran, in 2014. He is currently pursuing the Ph.D. degree with the Department of Mechanical Engineering, Iowa State University, where he is also a member of the System Reliability and Safety Laboratory. His research interests include engineering design under uncertainty and design for resilience.

Simon Laflamme received the M.Eng. degree in civil engineering and the Ph.D. degree in materials and structures from the Massachusetts Institute of Technology, Cambridge, MA, USA, in 2007 and 2011, respectively. He is currently an Associate Professor with the Department of Civil, Construction, and Environmental Engineering, Iowa State University, Ames, IA, USA, where he is also the Associate Director of the Center for Nondestructive Evaluation. His research interests include structural health monitoring and control.

Chao Hu received the B.E. degree in engineering physics from Tsinghua University, Beijing, China, in 2007, and the Ph.D. degree in mechanical engineering from the University of Maryland at College Park, College Park, MD, USA, in 2011. He was a Principle Scientist with Medtronic, Inc., MN, USA, from 2011 to 2015. He is currently an Assistant Professor with the Department of Mechanical Engineering, Iowa State University, Ames, IA, USA. His research interests include reliability-based design and prognostics.